

Analytical investigation of Buckling Restrained Braces' applications in bidirectional ductile end diaphragms for seismic performance of slab-on-girder bridge



Xiaone Wei^{a,*}, Michel Bruneau^b

^a Michael Baker International, Chicago, IL 60606, United States

^b Department of Civil, Structural, and Environmental Engineering, University at Buffalo, Amherst, NY 14260, United States

ARTICLE INFO

Article history:

Received 20 January 2017

Revised 15 March 2017

Accepted 18 March 2017

Available online 4 April 2017

Keywords:

Bidirectional ductile end diaphragm

Buckling Restrained Braces

Seismic analysis

Slab-on-girder bridges

Skew bridge

ABSTRACT

The AASHTO Guide Specifications for Seismic Bridge Design includes provisions for the design of ductile diaphragms as Permissible Earthquake-Resisting Elements (EREs) to resist seismic loads applied in the transverse direction of bridges. However, two major limitations for this system are that: (1) other lateral-load resisting strategies have to be combined with the transverse ductile diaphragms to address seismic excitations acting along the bridge's longitudinal axis; (2) the existing AASHTO provisions (reflecting the limits of existing research) only apply to straight bridges and provide no guidance on how to implement ductile diaphragms in skew bridges. This paper investigates ductile end diaphragm systems (EDSs) inserted in the slab-on-girder bridge superstructure, with Buckling Restrained Braces (BRBs) arrayed in two different bidirectional configurations so as to provide bi-directional resistance. Benchmark skew and straight bridge models were designed with both EDSs and analyzed using nonlinear time history analysis method to examine their seismic performance. Variations in skew, fundamental period of vibration, and earthquake excitation characteristics were considered. These dynamic analyses allowed investigating the impact of these parameters on global behavior, as well as understanding the magnitude of local demands and the extent of bidirectional displacements that the BRBs must be able to accommodate while delivering their ductile response. The long-term service life of BRBs installed across expansion joints and subjected to bridge thermal expansion histories was also studied and a minimum ratio of the BRB core length over the whole bridge length was recommended. For BRBs' design and implementation in EDSs, these analytical results can help predict a regime of relative end-displacements representative of the BRB's demands, when the bridge is subjected to both earthquake and temperature change in the superstructure.

© 2017 Elsevier Ltd. All rights reserved.

1. Introduction

Ductile diaphragms developed to reduce the seismic vulnerability of steel bridges have been analytically and experimentally studied in the past. To investigate the behavior of steel bridges during earthquakes, Zahrai and Bruneau [1] investigated the role of the diaphragms on the seismic behavior of slab-on-girder bridges having different length by comparing the behavior of bridges with and without diaphragms through pushover analysis. In Zahrai and Bruneau [2], ductile end diaphragms to be installed in the steel superstructure of slab-on-girder steel bridges was proposed as a seismic retrofit strategy. A design procedure for ductile end diaphragms

* Corresponding author.

E-mail address: xiaonewe@buffalo.edu (X. Wei).

was proposed using either shear links, Triangular-plate Added Damping and Stiffness Devices (TADAS), or Eccentric Braced Frame (EBF) placed in an inverted Y-bracing configuration in the ductile diaphragm. Zahrai and Bruneau [3] presented experimental results on full-scale ductile diaphragm specimens having three proposed configurations and subjected to conventional reversed cyclic inelastic loading as well as pseudo-dynamic testing. For deck-truss bridges, Sarraf and Bruneau [4] proposed a ductile seismic retrofit solution to improve its seismic vulnerability by introducing special ductile diaphragms to replace the end cross-frames and the lateral braces panels adjacent to the support. Computer simulation of the retrofitted deck-truss bridge model subjected to severe ground motions proved that the proposed end ductile diaphragm significantly enhanced the seismic performance of deck-truss bridges. In Sarraf and Bruneau [5], a performance based design procedure of the ductile diaphragm in deck-truss bridges was

proposed using shear links, TADAS, and EBF. Bruneau et al. [6] presented a step-by-step design procedure for specially detailed ductile diaphragms in slab-on-girder bridges and deck-truss bridges, based on the analytical and experimental work originally developed for retrofitted bridges in Zahrai and Bruneau [1–3], and Sarraf and Bruneau [4–5]. Design equations were provided for the systems with shear links, EBF and TADAS devices. Carden et al. [7–8] evaluated the performance of ductile end cross frames using single angle X and BRBs in a straight single-span two-girder bridge model with a scale factor of 0.4 from a bridge prototype. Both bridge models were tested using two actuators acting at the deck level of the bridge model by conducting reversed static load in its transverse direction and using shake table testing for increasing amplitudes of the 1940 El Centro earthquake ground motion applied in the transverse direction. Bridge models with both types of end diaphragms showed satisfactory ductile seismic response.

The AASHTO Guide Specifications for LRFD Seismic Bridge Design [9] includes provisions for steel bridges designed with specially detailed ductile diaphragms to resist seismic loads applied in the bridge transverse direction. Implementations of the ductile diaphragm concept still remain limited, because ductile diaphragms covered by AASHTO [9] can only be implemented in bridges without skew, and only provide resistance to earthquake excitations acting in the direction transverse to the bridge axis. The issues of skew and bi-directionality are serious limitations and real impediments to the implementation of ductile diaphragms, which is unfortunate because ductile diaphragms are a low-cost seismic solution compared to other alternatives. Celik and Bruneau [10] introduced the Bidirectional End Diaphragm System (EDS) inserted in straight or skew slab-on-girder bridge superstructures, to resist bidirectional earthquake excitations. Two schemes of bidirectional EDSs (i.e. geometrical layouts) were proposed as shown in Fig. 1, and BRBs were arrayed to provide ductile response to all horizontal seismic forces. Closed-form expressions were derived for both schemes to express stiffness, yield strength, yield displacement, and hysteretic energy dissipation as a function of a given ductility level. The effect of changing certain parameters in the closed-form hysteretic model was studied based on static pushover analyses. However, the adequacy of using bidirectional EDSs to improve bridge seismic performance when subjected to earthquake excitations was not investigated; this is needed to validate the bidirectional diaphragm concept for practical implementations.

This paper investigates a proposed design procedure for bidirectional EDSs to be able to explicitly address the fact that earthquake simultaneously shake a bridge in all horizontal directions (not just transversely to the bridge axis), and makes this solution also applicable to skew bridges (a large percentage of all bridges). BRBs were chosen here to serve as the diaphragm's Structural Fuses (SF), to protect other structural elements, because of their high effectiveness in dissipating hysteretic energy, leaving those protected elements with minimal damage or even intact. After the earthquake, BRBs are designed to be relatively easily removed and replaced. The repair of the bridge can be expedited in this sense, which fits in the objectives of Accelerated Bridge Construction (ABC) from a post-earthquake perspective. Note that other hysteretic energy dissipation devices may equally work for this purpose.

BRBs have been implemented in many buildings all around the world because of their stable hysteretic energy dissipation capability and ease of design. Analytical and experimental research work has proven the effectiveness of BRBs in reducing building frames' seismically-induced inelastic deformations (see Wada et al. [11], Aiken et al. [12], Clark et al. [13], Lopez et al. [14], among many for building applications). The applications of BRBs in bridge is relatively limited compared to those in buildings, but a few implementations can still be found (Usami et al. [15]; Kanaji et al. [16]; Reno and Pohl [17]; Oya et al. [18]; Lanning et al., [19]). A

new bridge shown in Uang et al. [20] was designed with the transverse ductile diaphragm using BRBs. More details and figures on the bridge applications of BRBs mentioned above can be found in Wei and Bruneau [21] and Uang et al. [20]. This past research demonstrated that BRBs can develop stable hysteresis when subjected to in-plane cyclic loading, provided the BRB's end connections are designed to ensure that BRBs can reach the design axial strength of their core plate without first developing instability issues at their ends. The out-of-plane instability of the BRB has been observed in several BRBF tests (Aiken et al. [22]; Roeder et al. [23]; Tremblay et al. [24], Tsai et al. [25]). Tsai et al. [25] reported the out-of-plane buckling of the gusset plate that connected a BRB to a column when a full-scale 3-story 3-bay BRBF reached 2% drift. Tsai and Hsiao [26] described the details of a gusset plate stiffened by adding edge stiffeners to improve the seismic performance of the BRBF. Hikino et al. [27] performed shake table tests on a single-story, single bay BRBF with BRBs in a chevron configuration. Two types of BRBs with different embedment length of the transition segment inside the steel casing were used in the test. The BRB with a longer transition segment embedment length exhibited better hysteretic behavior than the other.

Since the BRB application in bidirectional ductile diaphragms proposed here will require even larger out-of-plane displacement capacity than any BRB ever tested, the authors designed two types of BRBs end connection details and investigated their behavior by subjecting them to an extensive set of quasi-static experiments consisting of a regime of combined relative end displacement histories representative of the results predicted from the parametric analytical studies presented in this paper. The BRBs with both types of end connections were proven capable of resisting the different bidirectional displacement protocols considered. Information of this comprehensive experimental work and corresponding design and detailing recommendations will be presented in a future paper.

In this paper, the bridge and configurations of the two proposed types of bidirectional EDSs with BRBs are presented in Section 2. In Sections 3 and 4, design procedures are proposed for both EDSs in skew and non-skew bridges, and the corresponding properties of these bridges with EDSs are presented. In Sections 5 and 6, the ground motions are selected and scaled to perform the EDS-1 and EDS-2 bridges dynamic nonlinear time history analyses, and results from those analyses are examined to determine the impact of different parameters on the bridge's global behavior, as well as to understand the magnitude of local demands and the extent of bidirectional displacements that the BRBs must be able to accommodate while delivering their ductile response. In Section 7, the long-term service life of BRBs installed across expansion joints and subjected to bridge thermal expansion histories are also investigated.

2. Bidirectional EDSs and simplified bridge models

Two types of bidirectional EDSs, namely EDS-1 and EDS-2 (Fig. 1), are described as follows:

- (1) EDS-1: two pairs of structural fuses installed at each end of a span, in a configuration that coincides with the skew and longitudinal directions;
- (2) EDS-2: a single pair of structural fuses installed at each end of a span, at angles that do not coincide with the bridge longitudinal and skew directions.

A straight simply-supported single-span steel slab-on-girder bridge is considered as the prototype bridge in this study. The height of the girder in this bridge is 72", with center-to-center

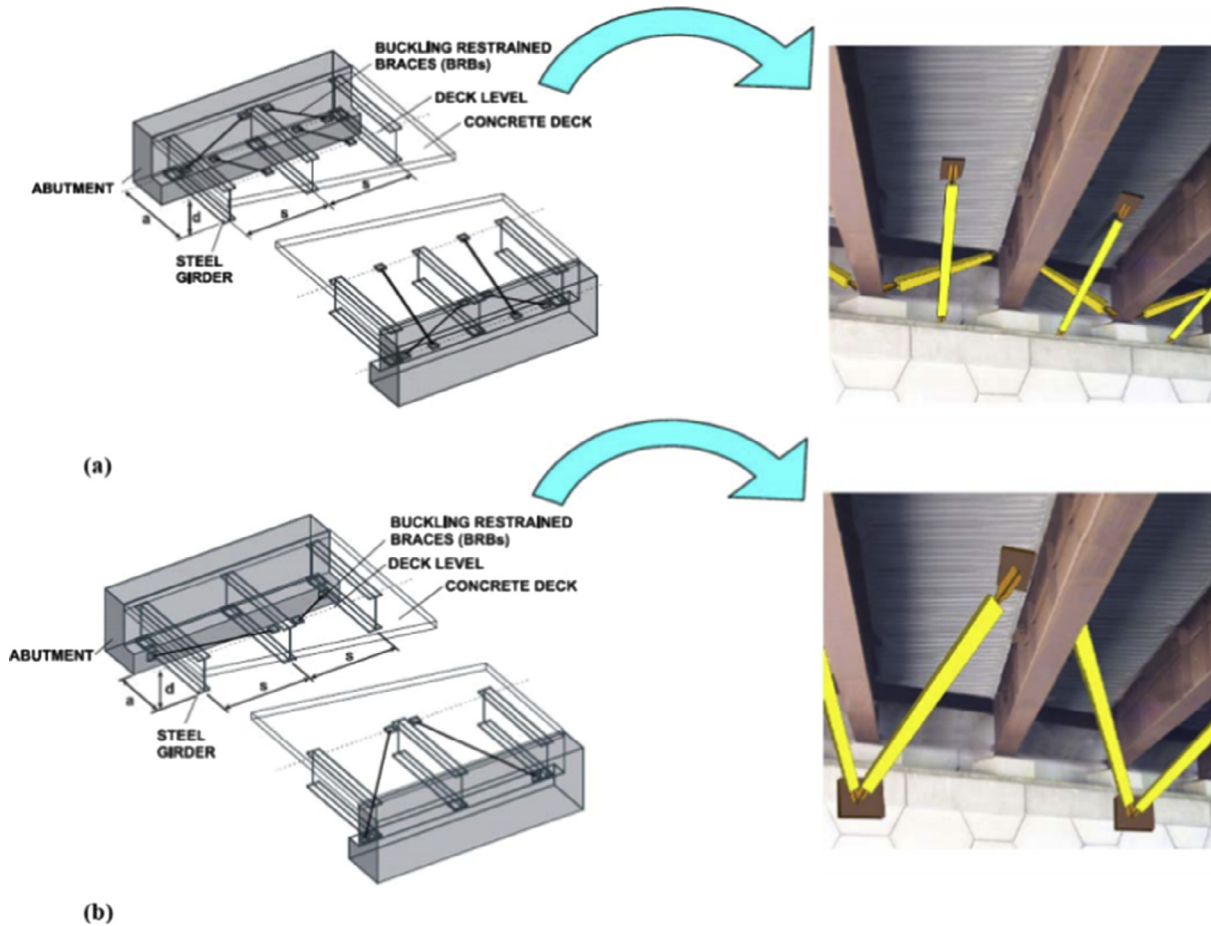


Fig. 1. Proposed Schemes for Bridge Ductile End Diaphragms: (a) EDS-1; (b) EDS-2.

space of 72". The deck is assumed to be supported on bidirectional sliding bearings or other bearings with negligible strength to horizontal deformations at the abutment. The bridge length is assumed to be 100 ft. The weight of the bridge (mg) is 2000 kips, and m is the mass of the bridge. The bidirectional EDSs with BRBs are implemented at both end of this prototype bridge. The corresponding simplified bridge models consider a rigid bridge deck as a floating span. The flexibility of the girder and slab is neglected, as well as the stiffness contribution from the bearing web stiffeners.

The key dimensions of the bidirectional EDSs are the girder skew spacing projection in the transverse direction, s , end diaphragm depth, d , which is approximately equal to the girder depth, and the horizontal longitudinal distance between connections of the longitudinal BRB at deck level and the abutment, a . The material in the steel core of BRB is assumed bilinear with yield stress, F_{yb} , and the Young's modulus, E .

Fig. 2a shows the simplified skew bridge with EDS-1, having equal skew angle, ϕ , of 45 degrees at the two ends of the bridge span. At the ends of the span, the thicker black lines in the enlarged view represent the structural elements used to model the EDS at both ends of the bridge, whereas the gray line are reference lines for an equivalent non-skew bridge. The lines with symbols represent the BRBs in the longitudinal and skew direction, and they can be visualized as the yellow structural members in Fig. 1. The other black lines at the bridge ends represent the rigid member used to complete the EDS (recall that girders are of a height " d ", spaced at " s " from each other, and that the BRBs project over a distance " a " along the axis of the bridge). The bridge superstructure is shown by a long thick black line in the x -direction connecting the

EDSs at the two ends in the global view of the bridge. The two supports at both ends of the bridge are at a skew angle from each other, which result in an unsymmetrical distribution of BRBs in 3D. Fig. 2b shows the corresponding non-skew (straight) bridge with EDS-1 at the two ends of the bridge span (enlarged view at one end); the symbol and construct is similar, but easier to visualize given the absence of skew. Figs. 3 and 5 are presented in similar ways to show the EDSs in the skew and non-skew (straight) bridges. The stiffness of the EDS-1 in Fig. 2b is K_L and K_T in the longitudinal and transverse directions, respectively. The yielding core length ratio, c , is the length of the BRB restrained yielding steel core over the length of the entire BRB. In EDS-1, c_{Lb} and c_{Sb} are for the longitudinal and skew/transverse BRBs, respectively. The lengths of the longitudinal, and the skew/transverse BRB are:

$$L_{Lb} = \sqrt{a^2 + d^2} \quad (1)$$

$$L_{Sb} = \sqrt{(s/\cos\phi)^2 + d^2} \quad (2)$$

Similarly, Fig. 3a shows the simplified skew bridge with EDS-2, having equal skew angle, ϕ , of 60 degrees at the two ends of the bridge span (enlarged view shown at one end). The stiffness of EDS-2 is K_L and K_T in the longitudinal and transverse directions, respectively. Fig. 3b shows the simplified non-skew bridge with EDS-2 at two ends of the bridge span (enlarged view at one end). The yielding core length ratio of the BRBs in the EDS-2 configurations is c_L and c_S for the long and short BRBs, respectively. The lengths of the longitudinal, and the short BRB are:

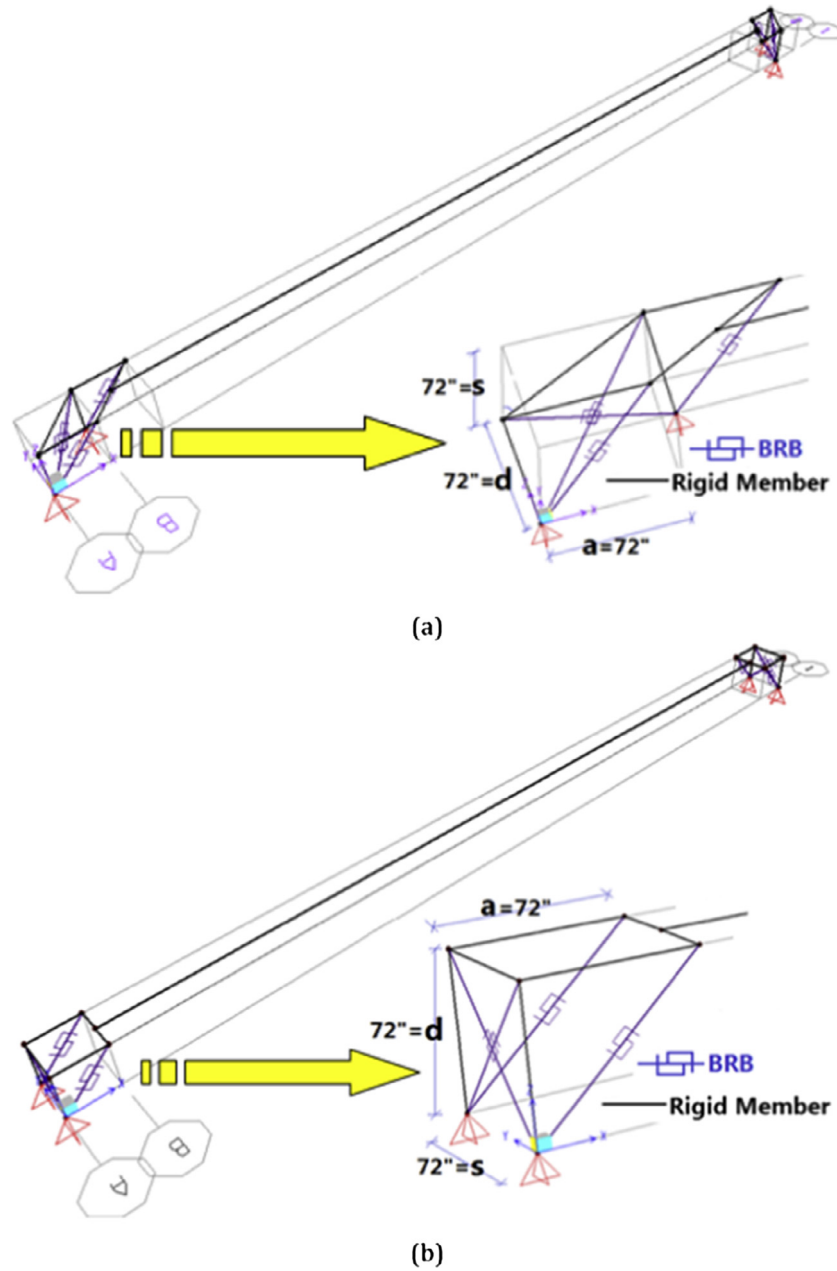


Fig. 2. EDS-1 bridge diaphragms with BRBs and enlarged view at the end: (a) skew 45° (b) skew 0°.

$$L_L = \sqrt{(a + s \times \tan\phi)^2 + s^2 + d^2} \tag{3}$$

$$L_S = \sqrt{(a - s \times \tan\phi)^2 + s^2 + d^2} \tag{4}$$

3. Proposed design procedures of bidirectional EDSs

Celik and Bruneau [10] discussed the seismic resistance of skewed steel bridges under bidirectional earthquake excitation for both EDS schemes through numerical nonlinear pushover analyses. To summarize:

- Lateral earthquake loads were applied at the deck level on the bidirectional EDSs in both longitudinal and transverse directions;

- The yielding sequence of BRBs was related to the ratios of applied lateral loads, the skew bridge angle ϕ , and the ratios of EDS dimensions d/a and d/s , and;
- Assuming equal areas of all the BRBs; the yield displacement and yield strength in both the longitudinal and transverse direction of the bidirectional EDS was expressed in terms of yield strength and displacement of individual BRB.
- In that study, no yield length ratios of BRBs were considered.

Following up on that work, the purpose of the study reported here was to investigate the bridge's seismic demands of the bidirectional EDSs by performing nonlinear time history analyses. For non-skew bridges, seismic response in the longitudinal and transverse direction is uncoupled. Per the response spectrum at the bridge location, the applied ground motions can be scaled to match the spectral seismic demand, which is related to the period of the bridge in either of the longitudinal or transverse directions. Thus,

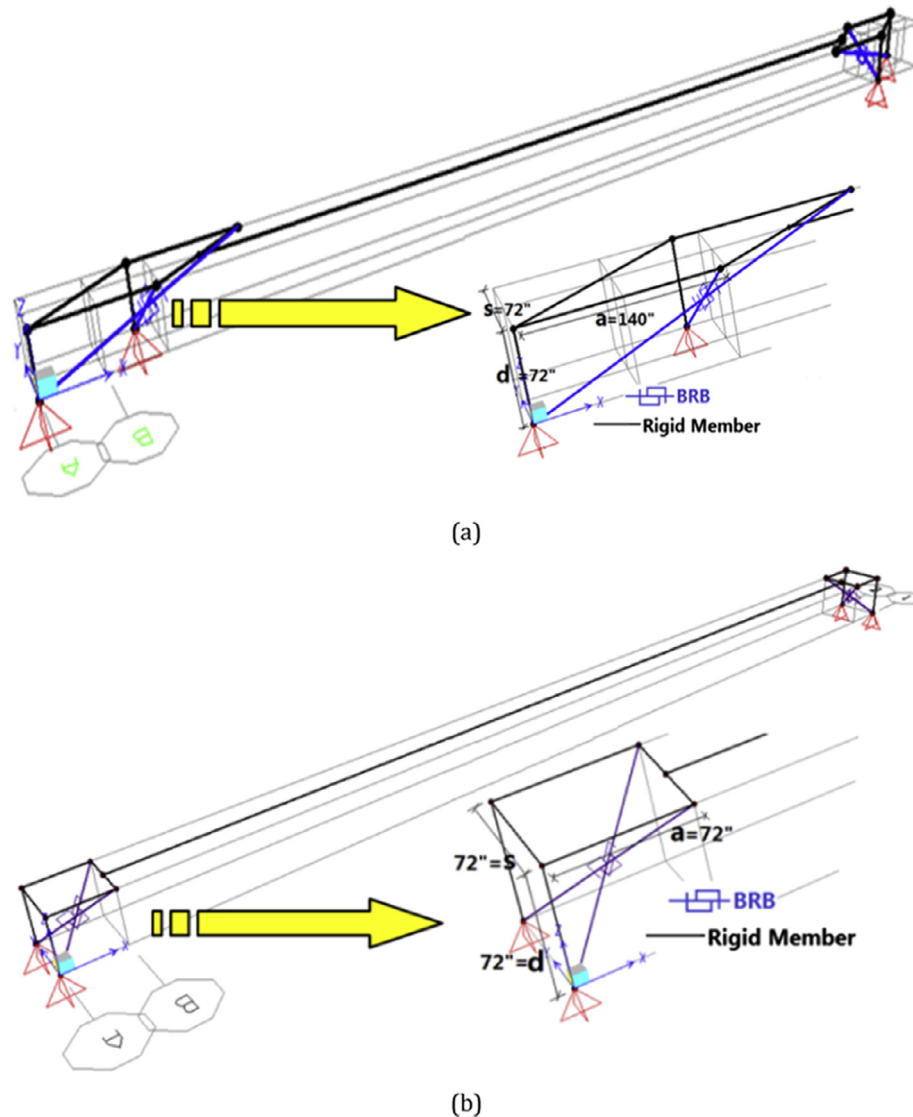


Fig. 3. EDS-2 bridge diaphragms with BRBs and enlarged view at the end: (a) skew 60° (b) skew 0°.

the displacement demands of the bridge can be calculated separately in the transverse or longitudinal directions. However, due to the complex skew bridge behavior related to the coupling of the BRBs' response, the main vibration directions of the skew bridge are not in the longitudinal and transverse directions. An approach was therefore taken here to design the skew bridges to have the same yield strength and yield displacement in the transverse and longitudinal directions as their equivalent non-skew bridge. The scaled ground motions used to analyze the non-skew bridge with EDSs were also used and applied to the skew bridges, and corresponding displacement demands in both the longitudinal and transverse directions were obtained. The magnification factors of skew bridges' displacement demands from the non-skew bridges were used in the prediction of the skew bridges' displacement demands in the design procedures of bidirectional EDSs.

For the simplified bridge models with both EDSs, the difference in the translational vibration directions and corresponding periods is also identified. The non-skew bridge vibrates translationally in the global longitudinal and transverse directions, while the skew bridges' translational periods and vibration directions depend on the bridge's skew angle, as well as the relative strength and stiffness between the longitudinal and skew BRBs (EDS-1 scheme) or between the long and short BRBs (EDS-2 scheme).

3.1. EDS-1 scheme

The periods of the non-skew equivalent bridge are first assumed as T_L and T_T in both the longitudinal and transverse direction, respectively. The stiffness of EDS-1 non-skew equivalent bridge in the longitudinal and transverse direction, K_L and K_T , are:

$$K_L = 2\pi\sqrt{m/T_L} \quad (5)$$

$$K_T = 2\pi\sqrt{m/T_T} \quad (6)$$

For the specified design acceleration response spectrum at the bridge location, the spectral acceleration at a given period T is S_a . Elastic force demand of the bridge, mS_a , can be obtained. Knowing the stiffness K calculated from the period T and the bridge mass m , the maximum elastic displacement demand, δ_u , is equal to mS_a/K , which was based on the assumption of "equal elastic and inelastic displacements for a given period" commonly used in earthquake resistant design (displacement magnification factors presented later in this paper also reflect this assumption). The displacement ductility demand is, μ , and the yield displacement of EDS-1 non-skew equivalent bridge is

$$\delta_y = mS_a/K\mu \quad (7)$$

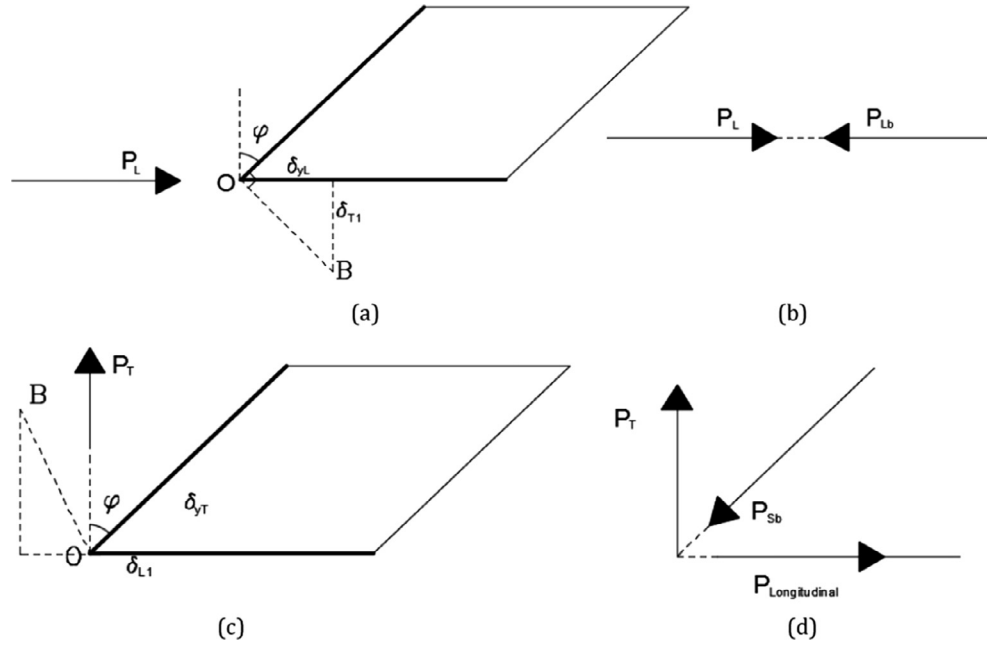


Fig. 4. Displacement compatibility and force equilibrium illustrated for EDS-1 configurations: force applied in the longitudinal direction (a) displacement compatibility (b) force equilibrium; force applied in the transverse direction (c) displacement compatibility (d) force equilibrium.

The yield displacements of the EDS-1 non-skew bridge in either the longitudinal or transverse direction, δ_{yL} and δ_{yT} , can be calculated from Eq. (7). The strength of EDS-1 non-skew equivalent bridge in the longitudinal and transverse direction, P_L and P_T are:

$$P_L = K_L \delta_{yL} \quad (8)$$

$$P_T = K_T \delta_{yT} \quad (9)$$

For a skew bridge with EDS-1, when the longitudinal force is applied to the bridge as shown in Fig. 4a and b, skew BRBs are not subjected to any force. The bridge's displacement occurs perpendicular to the skew direction. When longitudinal BRBs yield, the bridge's displacement in the global longitudinal direction is δ_{yL} . Due to the skewness, the corresponding displacement in the global transverse direction is

$$\delta_{T1} = \delta_{yL} \times \tan\varphi \quad (10)$$

The yield length ratio of the longitudinal BRB can be obtained as

$$c_{Lb} = \delta_{yL} \times (E \times a) / (a^2 + d^2) / F_{yb} \quad (11)$$

Note that the yield length ratio is typically smaller than 1.0.

The yield displacement and strength of the bridge in the transverse direction is dependent on the sequence of yielding of the BRBs, since the force applied in the transverse direction would put force in the BRBs in both the longitudinal and skew direction as shown in Fig. 4c and d. In the case considered here, skew BRBs were designed to yield first. When the skew BRB yield, the global transverse displacement is δ_{yT} . The corresponding displacement in the global longitudinal direction is

$$\delta_{L1} = K_T \delta_{yT} \times \tan\varphi / K_L \quad (12)$$

Note that this longitudinal displacement should be smaller than δ_{yT} . The yield length ratio of the skew BRB is calculated as:

$$c_{Sb} = \frac{\delta_{yT} \times Es \times (1 - K_T \times (\tan\varphi)^2 / K_L)}{((s / \cos\varphi)^2 + d^2) \times F_{yb}} \quad (13)$$

The total number of BRBs in the EDS-1 bridge is 4, which is the same in the longitudinal and skew direction, respectively. The yield strength of each longitudinal and skew BRB is

$$P_{Lb} = P_L \sqrt{a^2 + d^2} / (4a) \quad (14)$$

$$P_{Sb} = P_T \sqrt{(s/\cos\varphi)^2 + d^2} / (4s) \quad (15)$$

The corresponding yielding core area of the longitudinal and skew BRB would be P_{Lb}/F_{yb} and P_{Sb}/F_{yb} . The stiffness of the longitudinal and skew BRB are:

$$K_{Lb} = EP_{Lb} / (c_{Lb} F_{yb} L_{Lb}) \quad (16)$$

$$K_{Sb} = EP_{Sb} / (c_{Sb} F_{yb} L_{Sb}) \quad (17)$$

Fig. 5a shows the EDS-1 configuration with BRBs at one end of the bridge. The angle of the skew BRB with the horizontal plane is β_1 . The angle of the longitudinal BRB's projection in the horizontal plane with the x-axis is β_2 . In Fig. 5b, the stiffness in the longitudinal and skew direction, K_L and K_S , can be calculated as:

$$K_L = 2K_{Lb} \cos^2\beta_1 \quad (18)$$

$$K_S = 2K_{Sb} \cos^2\beta_1 \quad (19)$$

The ratio of stiffness K_L and K_S in the longitudinal and skew directions of EDS-1 bridge is ρ . Fig. 5b shows the relative longitudinal and skew directions in the EDS-1 configuration with the solid black lines representing the longitudinal and skew direction, respectively. The dashed line indicates the transverse direction in the EDS-1 configuration. The first two main vibration directions of EDS-1 bridge are T_1 and T_2 . The corresponding stiffness are K_1 and K_2 , and the directions of vibration are illustrated in Fig. 5b in dash-dot lines, which are perpendicular to each other. The angle

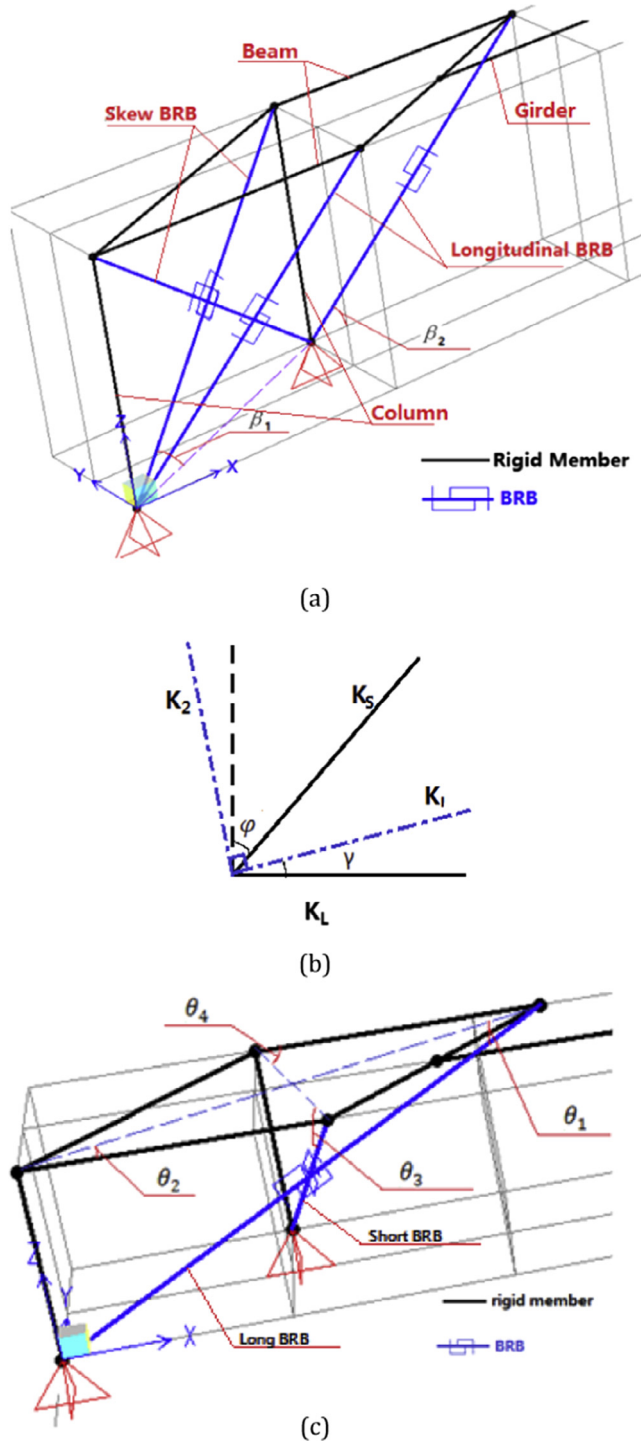


Fig. 5. Illustration in EDS configurations: (a) angles of BRBs in EDS-1; (b) vibration directions in EDS-1; (c) angles of BRBs in EDS-2.

γ , between the longitudinal and the main vibration direction corresponding to T_1 , is $(\pi/2 - \varphi)/(1 + \rho)$. The relationship between K_1 , K_2 , K_L and K_S is given as follows:

$$K_1 = K_L \times \cos^2\left(\frac{\pi/2 - \varphi}{1 + \rho}\right) + K_S \times \cos^2\left(\frac{\pi/2 - \varphi}{1 + \rho}\right)\rho \quad (20)$$

$$K_2 = K_L \times \sin^2\left(\frac{\pi/2 - \varphi}{1 + \rho}\right) + K_S \times \sin^2\left(\frac{\pi/2 - \varphi}{1 + \rho}\right)\rho \quad (21)$$

The periods corresponding to K_1 and K_2 are

$$T_1 = 2\pi\sqrt{m/K_1} \quad (22)$$

$$T_2 = 2\pi\sqrt{m/K_2} \quad (23)$$

3.2. EDS-2 scheme

The design of the EDS-2 bridge starts from the global yield strengths in the longitudinal and transverse direction, P_L and P_T , which are the same as for EDS-1 non-skew equivalent bridge. Here, the EDS at each end of the bridge has one long and one short BRB. Note that the global yield strength in either the longitudinal or transverse direction is obtained when there are only forces applied on the bridge in that direction.

The assumption made for the design of long BRBs is that long BRBs would yield first and short BRBs would remain elastic under the longitudinal force applied to the bridge. Therefore, when the force of P_L is applied gradually in the longitudinal direction of the bridge, the force demand on the long BRB will eventually reach its yield strength. This force that would produce yielding of the long BRB (i.e., for which BRBs would need to be designed) is related to the longitudinal force by:

$$P_{Lb} = P_L \times L_L / (4 \times a) \quad (24)$$

The corresponding force in the short BRB is

$$P_{short} = P_L \times L_S / (4 \times a) \quad (25)$$

By using the principle of virtual work, the global yield displacement in the longitudinal direction is

$$\delta_{yL} = 2(P_{Lb}^2 c_L L_L / (P_L A_L) + P_{short}^2 c_S L_S / (P_L A_S)) / E \quad (26)$$

Similarly, the short BRB would yield first and the long BRB would remain elastic under the transverse force applied to the bridge. When the force of P_T is applied gradually in the transverse direction of the bridge, the force demand on the short BRB will eventually reach its yield strength. The force that would produce yielding of the short BRB is related to the transverse force by:

$$P_{Sb} = P_T \times L_S \times (a + s \times \tan\varphi) / (4 \times s \times a) \quad (27)$$

The corresponding force in the long BRB is

$$P_{Long} = P_T \times L_L \times (a - s \times \tan\varphi) / (4 \times s \times a) \quad (28)$$

The global yield displacement in the transverse direction is

$$\delta_{yT} = 2(P_{Long}^2 c_L L_L / (P_T A_L) + P_{Sb}^2 c_S L_S / (P_T A_S)) / E \quad (29)$$

Note that P_{Long} and P_{short} are smaller than P_{Lb} and P_{Sb} .

With the yield displacements in the longitudinal and transverse direction known from the non-skew EDS-1 equivalent bridge, the yield length ratio of the long and short BRBs, c_L and c_S , can be obtained from Equations (26) and (29). The yielding core area of the long and short BRB would be P_{Lb}/F_{yb} and P_{Sb}/F_{yb} . The stiffness of the long and short BRB are:

$$K_{Long} = EP_{Lb} / (c_L F_{yb} L_L) \quad (30)$$

$$K_{Short} = EP_{Sb} / (c_S F_{yb} L_S) \quad (31)$$

In the simplified skew bridge model with EDS-2, the layout of long and short BRBs makes the response of the system coupled in the longitudinal and transverse direction. The equations of motion for free vibration of this kind of system are shown below, where K_{xy} and K_{yx} are not zero:

$$\begin{bmatrix} m & 0 \\ 0 & m \end{bmatrix} \begin{Bmatrix} \ddot{u}_x \\ \ddot{u}_y \end{Bmatrix} + \begin{bmatrix} K_{xx} & K_{xy} \\ K_{yx} & K_{yy} \end{bmatrix} \begin{Bmatrix} u_x \\ u_y \end{Bmatrix} = \begin{Bmatrix} 0 \\ 0 \end{Bmatrix} \quad (32)$$

Solving the eigenvalue problem for the dynamic equation in Eq. (32) would lead to the evaluation of the following equation:

$$\text{Det} \begin{bmatrix} K_{xx} - \omega^2 m & K_{xy} \\ K_{yx} & K_{yy} - \omega^2 m \end{bmatrix} = 0 \quad (33)$$

where: ω is the natural circular frequency of the system.

Eq. (33) gives the natural frequencies of the system:

$$\omega = \sqrt{\frac{K_{xx} + K_{yy} \pm \sqrt{(K_{xx} + K_{yy})^2 + 4(K_{xy}^2 - K_{xx}K_{yy})}}{2m}} \quad (34)$$

Therefore, the corresponding first two periods of vibration for translational modes are:

$$T_1 = \sqrt{\frac{8\pi^2 m}{K_{xx} + K_{yy} + \sqrt{(K_{xx} + K_{yy})^2 + 4(K_{xy}^2 - K_{xx}K_{yy})}}} \quad (35)$$

$$T_2 = \sqrt{\frac{8\pi^2 m}{K_{xx} + K_{yy} - \sqrt{(K_{xx} + K_{yy})^2 + 4(K_{xy}^2 - K_{xx}K_{yy})}}} \quad (36)$$

Similarly, in order to calculate the periods (T_1 , T_2), the values in the stiffness matrix (K_{xx} , K_{yy} , K_{xy}) need to be obtained first. Fig. 5c shows the EDS-2 configuration with BRBs at one end of the bridge. The angle of the long BRB with the horizontal plane is θ_1 . The angle of the long BRB's projection in the horizontal plane with the x-axis is θ_2 . The angle of the short BRB with the horizontal plane is θ_3 . The angle of the short BRB's projection in the horizontal plane with the x-axis is θ_4 . The stiffness of the long and short BRBs are K_{Long} and K_{Short} , respectively. The stiffness K_{xx} , K_{yy} , K_{xy} in Eqs. (32) and (33) can then be expressed as:

$$K_{xx} = 2(K_{Long} \cos^2 \theta_1 \cos^2 \theta_2 + K_{Short} \cos^2 \theta_3 \cos^2 \theta_4) \quad (37)$$

$$K_{yy} = 2(K_{Long} \cos^2 \theta_1 \sin^2 \theta_2 + K_{Short} \cos^2 \theta_3 \sin^2 \theta_4) \quad (38)$$

$$K_{xy} = 2(K_{Long} \cos^2 \theta_1 \cos \theta_2 \sin \theta_2 - K_{Short} \cos^2 \theta_3 \cos \theta_4 \sin \theta_4) \quad (39)$$

where K_{Short} and K_{Long} is the axial stiffness of the short and long BRB, respectively.

4. Simplified bridge model properties summary and modeling

For ease of comparisons for the displacement demands obtained from the nonlinear time history analyses, the EDS-1 skew bridge were designed to have the same yield strength and yield displacement in both longitudinal and transverse directions as the EDS-1 non-skew bridge. The skew angles of the bridges, φ , was contemplated to be changed at a 15-degree interval from 0 to 75 degree. Only 15 and 30 degree skews were considered for the EDS-1 skew bridges, since skew bridges with skew angles beyond 45 degrees could not be designed to have the equal yield strength and yield displacement as their equivalent EDS-1 non-skew bridge. The EDS-1 non-skew bridge is the equivalent bridge for the EDS-1 skew bridges of all skew angles. For the EDS-1 bridges shown in Fig. 2a and b, the three dimensions a , d , s are kept the same. Dimensions and properties of the EDS-1 in skew and non-skew bridges are tabulated in Table 1. Note that, in skew bridges, the cross section areas of the BRBs installed in the longitudinal and in the skew directions are not the same.

The skew and non-skew bridges with EDS-2 were designed to have the same yield strength and displacement in both the

Table 1
Properties of simplified skew and non-skew bridges with EDS-1.

| Bridge properties | Non-skew | Skew 15 | Skew 30 |
|--|----------|---------|---------|
| Skew angle (Degree) | 0 | 15 | 30 |
| First translational period T_1 (s) | 0.20 | 0.22 | 0.25 |
| Second translational period T_2 (s) | 0.20 | 0.17 | 0.12 |
| Stiffness in longitudinal direction (kip/in) | 5126.5 | 5126.5 | 5126.5 |
| Stiffness in skew direction (kip/in) | 5126.5 | 5919.6 | 10253.1 |
| Longitudinal BRB cross sectional area (in ²) | 9.00 | 9.00 | 9.00 |
| Skew BRB cross sectional area (in ²) | 9.00 | 9.16 | 9.72 |
| Global yielding displacement in both longitudinal and transverse directions (in) | 0.209 | 0.209 | 0.209 |
| Global yielding strength in both longitudinal and transverse directions (kips) | 1069.1 | 1069.1 | 1069.1 |
| Equivalent stiffness in both longitudinal and transverse directions (kip/in) | 5126.5 | 5126.5 | 5126.5 |
| Yielding length ratio of Longitudinal BRB | 1.00 | 1.00 | 1.00 |
| Yielding length ratio of skew BRB | 1.00 | 0.90 | 0.57 |

longitudinal and transverse direction as the bridges with EDS-1. For the skew and non-skew bridges with EDS-2 shown in Fig. 3a and b, the parameter s and d are the same, while the parameter a changes as the skew angle changes. The same a value cannot be used to design the skew bridge with EDS-2 to have the same yield strength and displacement as the EDS-2 equivalent non-skew bridge. Dimensions and properties of the EDS-2 in skew and non-skew bridge are tabulated in Table 2. Note that in skew bridges, the cross section areas of the long and short BRBs are not the same. It is acknowledged that, for skew bridges with skew angle beyond 60 degrees, the length of the BRBs may be too long to be practical; such large skew angles for EDS-2 were only considered here to show that EDS-2 systems can be theoretically designed to have equal yield displacement and yield strength in the longitudinal and transverse directions at large skew angles.

Since the periods of the equivalent non-skew bridges in the above cases all fall on the plateau of the average acceleration response spectrum considered, the 30-degree skew bridges with both EDS schemes were redesigned to have equivalent non-skew bridge periods of 0.5 s, 1.0 s, and 1.5 s, by keeping the same mass of the bridge and by changing the size of the BRBs. The properties of EDS-1 skew bridges of 30 degrees and corresponding equivalent non-skew bridges of 0.5 s, 1.0 s, and 1.5 s periods are shown in Table 3. Case 1, Case 2, and Case 3 in Table 3 each include a skew bridge and its equivalent non-skew bridge with periods corresponding to 0.5 s, 1.0 and 1.5 s, respectively. Note that for each case of bridges in Table 3, the stiffness of the skew bridge is tabulated in the longitudinal and skew direction, and its stiffness in the longitudinal and transverse directions are the same as those for the non-skew equivalent bridge in the same directions. Similarly, the properties of the EDS-2 skew bridges of 30 degrees and corresponding equivalent non-skew bridges of 0.5 s, 1.0 s, and 1.5 s periods are shown in Table 4.

The enlarged view of one end in the EDS-1 non-skew bridge model in Fig. 5a is used to illustrate how the model is built in *OpenSees*, Version 2.4.6 [28]. The girder line represents the superstructure of the simplified bridge model. The beam and columns are rigid members that connect the girder, BRBs, and the base. The bridge mass is distributed along the whole length of the girder. The girder and beam are defined by using the element command *rigidLink*(beam) to make the members rigid and create a rigid diaphragm. The columns, which serve as the links between the base and the top of the diaphragm, were modeled using the element command *rigidLink*(bar). BRB members were built by using the element command *truss*, and the material of BRBs was defined to be bilinear. Note that the BRB's actual hysteretic behavior exhibited a more complex behavior, including strain hardening and Bauschinger effect. A material modeling able to replicate the actual

Table 2
Properties of simplified non-skew and skew bridges with EDS-2.

| Bridge properties | Non-skew | Skew 15 | Skew 30 | Skew 45 | Skew 60 |
|--|----------|---------|---------|---------|---------|
| Skew angle (Degree) | 0 | 15 | 30 | 45 | 60 |
| a (in) | 72 | 72 | 75 | 95 | 140 |
| First translational period T_1 (s) | 0.200 | 0.213 | 0.221 | 0.212 | 0.206 |
| Second translational period T_2 (s) | 0.200 | 0.186 | 0.180 | 0.186 | 0.193 |
| Long-BRB cross sectional area (in ²) | 11.023 | 12.088 | 13.133 | 13.103 | 12.892 |
| Short-BRB cross sectional area (in ²) | 11.023 | 12.850 | 14.723 | 16.220 | 17.208 |
| Global yielding displacement in both longitudinal and transverse directions (in) | 0.209 | 0.209 | 0.209 | 0.209 | 0.209 |
| Global yielding strength in both longitudinal and transverse directions (kips) | 1069.1 | 1069.1 | 1069.1 | 1069.1 | 1069.1 |
| Yielding stress of material in BRBs' core in both directions (ksi) | 42 | 42 | 42 | 42 | 42 |
| Yielding length ratio of Long BRB | 0.67 | 0.63 | 0.61 | 0.59 | 0.47 |
| Yielding length ratio of Short BRB | 0.67 | 0.87 | 0.99 | 0.99 | 0.99 |

Table 3
Properties of simplified skew 30 degree bridges and corresponding equivalent non-skew bridges with EDS-1.

| Bridge properties | Case 1–0.5 s | | Case 2–1.0 s | | Case 3–1.5 s | |
|--|--------------|----------|--------------|----------|--------------|----------|
| | Skew | Non-skew | Skew | Non-skew | Skew | Non-skew |
| First translational period T_1 (s) | 0.62 | 0.50 | 1.24 | 1.00 | 1.87 | 1.50 |
| Second translational period T_2 (s) | 0.31 | 0.50 | 0.61 | 1.00 | 0.92 | 1.50 |
| Stiffness in longitudinal direction (kip/in) | 818.2 | 818.2 | 204.5 | 204.5 | 90.9 | 90.9 |
| Stiffness in skew (Transverse for nonskew) direction (kip/in) | 1636.4 | 818.2 | 409.1 | 204.5 | 181.8 | 90.9 |
| Longitudinal BRB cross sectional area (in ²) | 1.44 | 1.44 | 0.36 | 0.36 | 0.16 | 0.16 |
| Skew (Transverse for nonskew) BRB Cross Sectional Area (in ²) | 1.55 | 1.44 | 0.39 | 0.36 | 0.17 | 0.16 |
| Global yielding displacement in both longitudinal and transverse directions (in) | 0.209 | 0.209 | 0.209 | 0.209 | 0.209 | 0.209 |
| Global yielding strength in both longitudinal and transverse directions (kips) | 170.6 | 170.6 | 42.6 | 42.6 | 18.9 | 18.9 |
| Yielding length ratio of Longitudinal BRB | 1.00 | 1.00 | 1.00 | 1.00 | 1.00 | 1.00 |
| Yielding length ratio of Skew BRB | 0.57 | 1.00 | 0.57 | 1.00 | 0.57 | 1.00 |

Table 4
Properties of simplified skew 30 degree bridges and corresponding equivalent non-skew bridges with EDS-2.

| Bridge properties | Case 1–0.5 s | | Case 2–1.0 s | | Case 3–1.5 s | |
|--|--------------|----------|--------------|----------|--------------|----------|
| | Skew | Non-skew | Skew | Non-skew | Skew | Non-skew |
| First translational period T_1 (s) | 0.55 | 0.50 | 1.10 | 1.00 | 1.65 | 1.50 |
| Second translational period T_2 (s) | 0.44 | 0.50 | 0.89 | 1.00 | 1.33 | 1.50 |
| Stiffness in Longitudinal direction (kip/in) | 818.2 | 818.2 | 204.5 | 204.5 | 90.9 | 90.9 |
| Stiffness in transverse direction (kip/in) | 818.2 | 818.2 | 204.5 | 204.5 | 90.9 | 90.9 |
| Long BRB cross sectional area (in ²) | 2.10 | 1.76 | 0.52 | 0.44 | 0.23 | 0.19 |
| Short BRB cross sectional area (in ²) | 2.35 | 1.76 | 0.59 | 0.44 | 0.26 | 0.19 |
| Global yielding displacement in both longitudinal and transverse directions (in) | 0.209 | 0.209 | 0.209 | 0.209 | 0.209 | 0.209 |
| Global yielding strength in both longitudinal and transverse directions (kips) | 170.6 | 170.6 | 42.6 | 42.6 | 18.9 | 18.9 |
| Yielding length ratio of Long BRB | 0.61 | 0.67 | 0.61 | 0.67 | 0.61 | 0.67 |
| Yielding length ratio of Short BRB | 1.00 | 0.67 | 1.00 | 0.67 | 1.00 | 0.67 |

BRB's hysteretic behavior (i.e., model Steel02 in *OpenSees*) was used in the bridge model to perform the nonlinear time history analyses, the resulting displacement responses were compared with the case using bilinear material. It was found that the displacement demands obtained from using bilinear material were larger and thus conservative to use.

The total bridge length remains the same for all benchmark simplified bridge models, since the superstructure was assumed rigid and the length of the bridge does not affect the dynamic behavior of the bridges in this case. Modal and pushover analyses were performed in *OpenSees*, and verified with the equations that are used to calculate yield strength, yield displacement, and periods of the EDSs as presented in the Tables 1–4 by using the equations above.

5. Ground motions and scale factors for EDS-1 non-skew bridge

Nonlinear time history analyses of the skew and non-skew bridges were conducted by inputting orthogonal components of the ground motions records in the global longitudinal and transverse direction of each bridge, to investigate their inelastic displacement demands. The 44 ground motions specified in

FEMA-P695 [29] were used to perform the nonlinear time history analyses. Note that although the ground motions recommended by FEMA-P695 were developed for studies on building structures, using the same set of 44 ground motions from FEMA P-695 was adequate here as it provided a broad variability of ground motions, in order to generate the displacement response of the bridge with BRBs in the directional ductile end diaphragms.

For the non-skew bridge with EDS-1, the EDS behaviors in the two orthogonal directions are uncoupled and the system can be detailed to behave in the bilinear manner shown in Fig. 6a (neglecting the lateral stiffness of the steel girders in this application). The EDSs' displacement limits in both directions can translate into maximum global ductility demands, μ , themselves related to yielding displacement of the BRBs in the EDSs. The maximum ground motions scaling factor was calculated to correspond to the target global displacement ductility. To ensure that those ductility demands are not exceeded during nonlinear time history analyses, relationships must be established between these ductility values and the minimum yield strength of the system, V_y , itself related to $V_{elastic}/R$, where $V_{elastic}$ is the corresponding elastic force demand. Different relationships between R , μ , and the bridge's

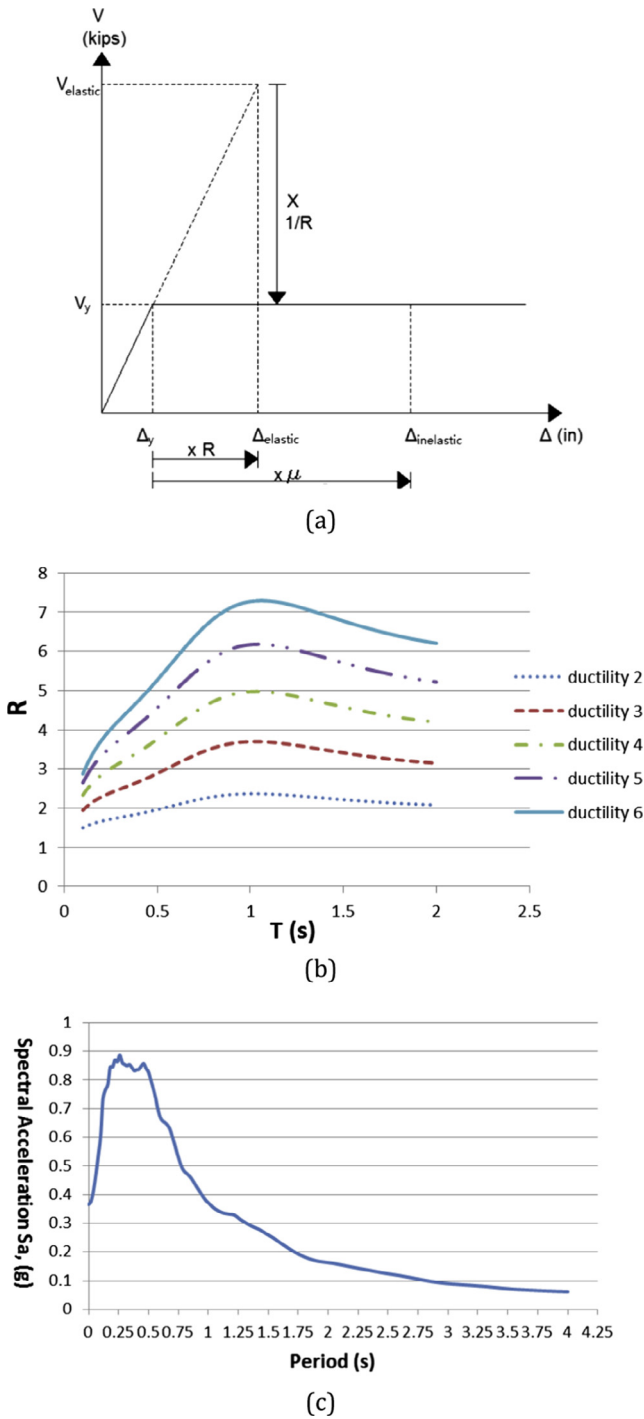


Fig. 6. (a) Illustration of displacement ductility and force reduction factor for bilinear system; (b) The relationship between R and T for a certain ductility; (c) The average acceleration response spectrum of 44 ground motions.

modal period T can be found in Miranda and Bertero [30], such as in Eqs. (40) and (41) (referenced by MCEER/ATC49 [31]). For a certain ductility μ ranging from 2 to 6, the force reduction factor R varies as a function of T as shown in Fig. 6b. The average spectral acceleration of the scaled 44 ground motions, shown in Fig. 6c, at the bridge modal period in each direction corresponds to the elastic force demand S_{a^e} , and all the 44 ground motions use the same scale factor of $V_y R / (m S_a)$.

$$R = \frac{\mu - 1}{\phi} + 1 \geq 1 \quad (40)$$

$$\phi = 1 + \frac{1}{12T - \mu T} - \frac{2}{5T} \exp \left[-2 \left(\ln T - \frac{1}{5} \right)^2 \right] \quad (41)$$

As mentioned above, the EDS-1 non-skew bridge's response in the transverse and longitudinal direction is uncoupled, therefore, the bilinear system behaviors in these two directions were used to assess the relationship between R and μ . The scaled ground motions calculated above were applied to the EDS-1 equivalent non-skew bridge to investigate whether the displacement demand would exceed the assumed target displacement. The inelastic displacement demands of the EDS-1 non-skew bridges with different periods were compared with the assumed target displacements (taken as equal to the yield displacement times the target ductility μ in this case); results of this comparison were used to define the inelastic displacement magnification factor, R_{dl} . This factor is similar to the displacement magnification for short period bridges provided by Equation 4.3.3 in AASHTO [9]. Various non-skew equivalent EDS-1 with translational periods ranging from 0.2 s to 1.5 s were analyzed. Target ductilities from 2 to 6 were used. Table 5a shows the force reduction factor R corresponding to the ductilities for each period from the non-skew equivalent bridges with EDS-1s. For example, for the EDS-1 non-skew bridge having the period of 0.3 s, the force reduction factor obtained from Eqs. (40) and (41) is 3.15 for the target ductility of 4. Due to the page limit, except for the non-skew bridge with EDS-1 of 0.2 s, 0.5 s, 1.0 s, and 1.5 s periods (Tables 1–4), the properties for the rest of EDS-1 s in the non-skew bridge considered in Table 5a are not presented and can be found in Wei and Bruneau [21].

Table 5b presents the design yield displacement of the non-skew equivalent bridge in the direction which corresponds to each period presented in Table 5a. The resulting average of the maximum displacement demands were obtained from nonlinear time history analyses using 44 ground motions and tabulated for all the ductilities from 2 to 6. Fig. 7 shows by how much (in percentage) the average displacements of the EDS-1 non-skew bridge (for all 44 ground motions) exceeds the assumed displacements limit of all ductility cases (from 2 to 6), as a function of the force reduction factor used. As the ductility increases, the percentage of exceedance typically increases. The smaller the force reduction factor, the smaller the percentage of exceedance of the resulting displacements from the estimated displacements. For periods around 1.0 s, the percentage of exceedance is generally larger than for the other periods. In all cases, the percentage of exceedance is less than 40% for the range of R between 1.5 and 7.5, which indicates that AASHTO equations gives much larger and more conservative value of R_d for short periods.

6. Displacement comparisons between skew and non-skew bridges

For the skew bridges with EDS-1 schemes presented in Table 1, their equivalent non-skew bridge with EDS-1 is the non-skew bridge in the same table. The ground motions applied in the longitudinal and transverse directions of the skew bridge were the same as those used for its equivalent non-skew bridge with the same scaling factors. The resulting average of the maximum displacements of the bridges with EDS-1s from analyses using 44 ground motions are shown in Table 5. The EDS-1 skew bridges' displacement demands were compared with those from the EDS-1 non-skew bridge cases in Table 6. The resulting longitudinal displacements of the skew bridges are generally larger than those for the equivalent non-skew bridges. The difference between the transverse displacements is smaller than that in longitudinal directions. For greater skew angle, the difference in longitudinal displacements is larger, with values up to 36% greater for the skew bridge.

Table 5a
Force reduction factor R for each period from the non-skew equivalent bridges with EDS-1s.

| Ductility | Period (s) | | | | | | | | | | | | | |
|-----------|------------|------|------|------|------|------|------|------|------|------|------|------|------|------|
| | 0.20 | 0.21 | 0.26 | 0.28 | 0.30 | 0.35 | 0.45 | 0.50 | 0.53 | 0.66 | 1.00 | 1.07 | 1.32 | 1.50 |
| 2 | 1.67 | 1.68 | 1.73 | 1.75 | 1.76 | 1.81 | 1.90 | 1.96 | 2.00 | 2.16 | 2.37 | 2.36 | 2.29 | 2.22 |
| 3 | 2.29 | 2.32 | 2.41 | 2.46 | 2.48 | 2.57 | 2.77 | 2.89 | 2.95 | 3.27 | 3.70 | 3.69 | 3.55 | 3.41 |
| 4 | 2.85 | 2.90 | 3.04 | 3.11 | 3.15 | 3.28 | 3.58 | 3.76 | 3.86 | 4.32 | 4.97 | 4.97 | 4.77 | 4.58 |
| 5 | 3.34 | 3.40 | 3.59 | 3.69 | 3.75 | 3.93 | 4.33 | 4.56 | 4.69 | 5.30 | 6.17 | 6.18 | 5.94 | 5.70 |
| 6 | 3.73 | 3.82 | 4.06 | 4.18 | 4.26 | 4.49 | 4.98 | 5.27 | 5.43 | 6.18 | 7.27 | 7.29 | 7.04 | 6.77 |

Table 5b
Yield displacement and displacement demand from nonlinear time history analyses of non-skew equivalent bridges with EDS-1s (Unit: in)

| Periods(s) | Yield Displacement | Ductility | | | | | |
|------------|--------------------|-----------|-------|-------|-------|-------|--|
| | | 2 | 3 | 4 | 5 | 6 | |
| 0.20 | 0.209 | 0.391 | 0.662 | 0.983 | 1.336 | 1.637 | |
| 0.21 | 0.231 | 0.418 | 0.674 | 1.004 | 1.369 | 1.735 | |
| 0.26 | 0.304 | 0.479 | 0.778 | 1.22 | 1.668 | 2.099 | |
| 0.28 | 0.209 | 0.347 | 0.595 | 0.876 | 1.155 | 1.419 | |
| 0.30 | 0.223 | 0.361 | 0.606 | 0.88 | 1.184 | 1.477 | |
| 0.35 | 0.469 | 0.768 | 1.175 | 1.701 | 2.259 | 2.808 | |
| 0.45 | 0.391 | 0.646 | 1.02 | 1.456 | 1.819 | 2.2 | |
| 0.50 | 0.209 | 0.335 | 0.526 | 0.734 | 0.992 | 1.21 | |
| 0.53 | 0.843 | 1.521 | 2.359 | 3.47 | 4.502 | 5.363 | |
| 0.66 | 0.717 | 1.299 | 2.054 | 3.034 | 4.003 | 4.786 | |
| 1.00 | 0.209 | 0.441 | 0.782 | 1.147 | 1.422 | 1.681 | |
| 1.07 | 1.613 | 3.435 | 6.173 | 8.637 | 10.82 | 13.23 | |
| 1.32 | 2.436 | 4.926 | 7.838 | 10.62 | 13.12 | 15.97 | |
| 1.50 | 0.209 | 0.385 | 0.589 | 0.77 | 1.009 | 1.249 | |

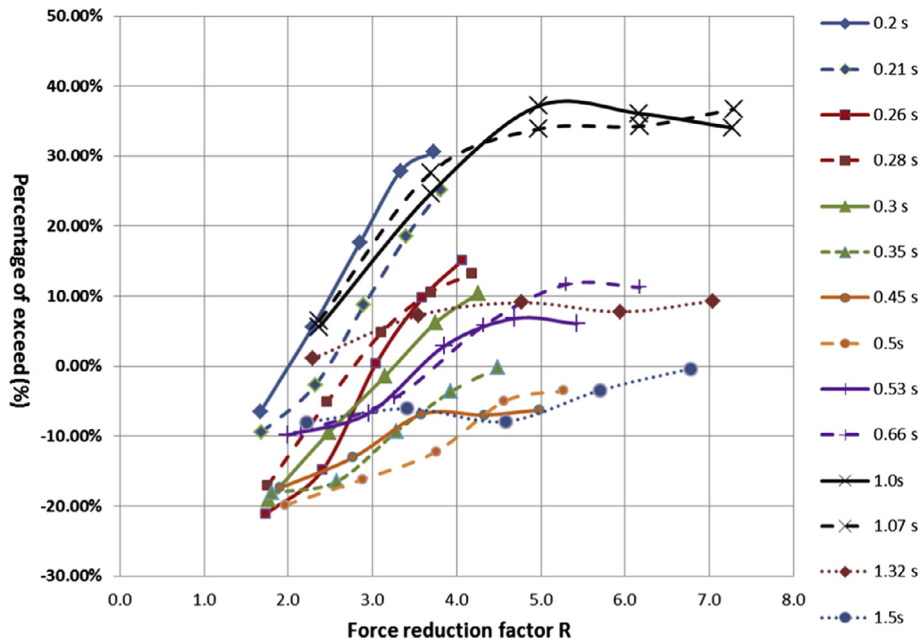


Fig. 7. Percentage of exceedance of non-skew bridge displacements from displacement limits versus the force reduction factors for 44 ground motions at various periods.

Table 6
Displacement demands and comparisons of the EDS-1 skew bridge and their equivalent non-skew bridges of period 0.2 s

| Ductility | Non-skew Longitudinal & Transverse | Skew 15° | | | | Skew 30° | | | |
|-----------|---------------------------------------|--------------|--------|------------|--------|--------------|--------|------------|--------|
| | | Longitudinal | | Transverse | | Longitudinal | | Transverse | |
| 2 | 0.391" | 0.415" | 6.19% | 0.397" | 1.56% | 0.531" | 35.84% | 0.418" | 6.98% |
| 3 | 0.662" | 0.677" | 2.27% | 0.646" | -2.40% | 0.853" | 28.84% | 0.666" | 0.57% |
| 4 | 0.983" | 0.982" | -0.14% | 0.914" | -7.04% | 1.199" | 21.95% | 0.973" | -0.99% |
| 5 | 1.336" | 1.300" | -2.71% | 1.250" | -6.44% | 1.509" | 12.94% | 1.276" | -4.48% |
| 6 | 1.637" | 1.571" | -4.06% | 1.556" | -4.97% | 1.757" | 7.32% | 1.583" | -3.29% |

The same comparisons were made to investigate the effect of period change on the difference in the displacement response between the skew and non-skew bridges with EDS-1 in Table 3. All the resulting displacement demands are shown in Table 7a with Case 1, Case 2, and Case 3 corresponding to the skew bridges mentioned in Table 3. The difference between the displacement demands of the EDS-1 skew and non-skew bridge are tabulated in Table 7b, which are smaller than those for the corresponding reference 30-degree skew bridge (i.e. with equivalent non-skew bridge period of 0.2 s) in Table 6. Generally, the longitudinal displacement results for skew bridges exceeded those from the non-skew bridge, with smaller maximum exceedance percentage as the period increased. The comparison of transverse displacements exhibited no specific trends as the period changed. At the period of 1.0 s, the percentage of transverse displacement response for skew bridge exceeded that of their corresponding equivalent non-skew bridge, which was the largest of all the 30-degree skew cases considered.

The non-skew bridges with EDS-2 in Table 2 had the same translational period of 0.2 s in the longitudinal and transverse directions as the non-skew bridges with EDS-1. Since the bridges with EDS-2 in Table 2 were designed to have the same strength and stiffness in the longitudinal and transverse directions as the bridges in Table 1, the ground motions' scale factors for bridges with EDS-2 were the same as the bridges with EDS-1 for all ductility considered. Table 8a shows the slight difference in the resulted average displacements between the non-skew bridges with EDS-2 and EDS-1.

The EDS-2 skew bridges were analyzed by applying in the same directions the same scaled ground motions used in the analyses of the non-skew bridges with EDS-2. The resulting displacement demands of the EDS-2 bridges are shown in Table 8b, and the displacements of the skew bridges are compared with those from the non-skew bridge with EDS-2 in Table 8c. The resulting longitudinal displacements of the EDS-2 skew bridges are generally less than those from the equivalent EDS-2 non-skew bridges, except for the 15 and 30-degree skew bridges. With increase of the skew angle, the displacement differences reduced, which is different than what was observed for the bridge cases with EDS-1. The greatest difference in the resulting displacements is 27.3% in the transverse direction for the 15-degree skew bridge from the non-skew bridge.

Similarly to what was done for the bridges with EDS-1, the displacement demands were obtained to investigate the effect of period change on the difference in the displacement response between the skew and non-skew bridges with EDS-2 as shown in Table 9a. Case 1, Case 2, and Case 3 in Table 9a each correspond to the bridges cases in Table 4. The same comparisons were made between the EDS-2 skew and equivalent non-skew bridges in Table 9b. It is found that the resulting EDS-2 skew bridges displacements are all smaller than that of their corresponding non-skew bridges.

In general, the displacement magnification factor for skew bridge, to apply to the displacement response of the equivalent non-skew bridges, R_{d2} , vary for the different EDS schemes as a function of skew angles. The difference may be a consequence of the difference in the true period of the skew and non-skew bridges, which would cause the variability in the inelastic displacements. Results of the above parametric studies indicate that, for skew bridges with skew angles smaller than 15 degrees, R_{d2} could be taken as 1.1 and 1.3 for EDS-1 and EDS-2, respectively. For skew bridges with skew angles larger than 30 degrees, R_{d2} could be taken as 1.4 and 1.15 for EDS-1 and EDS-2, respectively. For skew angle beyond 45 degrees, only the EDS-2 scheme is possible to achieve such that the yield strength and yield displacement of the skew and non-skew bridge are the same. Note that beyond 60-degree skew, the EDS-2 scheme would require BRB lengths that may not be practical.

Note that, for a bridge with designed EDS, it is possible and recommended here to design BRBs such that the EDS's fundamental period, T_{eff} , is the same in both the longitudinal and transverse direction. For a skew bridge, that would be the value for an equivalent non-skew EDS. For the bridge with skewness, the skew EDS would be designed to have the same yield strength and displacement as its equivalent non-skew EDS. In such a case the elastic force demand of the bridge is mS_a , for the specified design acceleration response spectrum at the bridge location. The yield strength of the non-skew EDS, V_y , is mS_a/R , and the stiffness, K_{eff} , is $4\pi^2m/T_{eff}^2$, and the yield displacement of the EDS, δ_y , is V_y/K_{eff} . The desired displacement ductility of the non-skew bridge EDS, μ , could be taken as the maximum value of 6 provided per Equation 4.3.3 in AASHTO [9]. Based on the above findings, the resulting inelastic displacement demand of the non-skew EDS would then be the elastic spectral displacement, $\delta_y\mu$, times the inelastic displacement magnification factor, R_{d1} , which is defined as 1.4 (per results presented in Fig. 7). The displacement demand of the skew EDS, δ_u , would then be calculated as $\delta_y\mu R_{d1}R_{d2}$, where R_{d2} is a displacement magnification factor relating the expected maximum displacement response of the skew bridge to that of its equivalent non-skew bridge, as summarized above.

7. Thermal effect on low-cycle fatigue of BRBs

Thermal movements (elongation and shortening) of the bridge superstructure resulting from temperature changes would impose displacement demands on the longitudinal BRBs connecting the superstructure to the abutments across expansion joints as shown in Fig. 8. The concern was whether the longitudinal BRBs can accommodate thermal expansion movements without the need for special detailing (i.e., in series with lock-up devices that allow thermal expansion under normal conditions, but engage the BRBs during the earthquakes). This issue was investigated by calculating the low-cycle fatigue life of longitudinal BRBs due to thermal movements of the bridge superstructure resulting from temperature

Table 7a
Displacement demands of the skew bridge and their equivalent non-skew bridges with EDS-1of increased periods (Unit: in).

| Ductility | Case 1 | | | Case 2 | | | Case 3 | | |
|-----------|----------|-------|-------|----------|-------|-------|----------|-------|-------|
| | Non-skew | | Skew | Non-skew | | Skew | Non-skew | | Skew |
| | L&T | L | T | L&T | L | T | L&T | L | T |
| 2 | 0.335 | 0.347 | 0.342 | 0.441 | 0.453 | 0.523 | 0.385 | 0.359 | 0.403 |
| 3 | 0.526 | 0.512 | 0.545 | 0.782 | 0.751 | 0.893 | 0.589 | 0.560 | 0.615 |
| 4 | 0.734 | 0.701 | 0.752 | 1.147 | 1.044 | 1.262 | 0.770 | 0.731 | 0.810 |
| 5 | 0.992 | 0.897 | 0.964 | 1.422 | 1.328 | 1.567 | 1.009 | 0.931 | 1.032 |
| 6 | 1.210 | 1.083 | 1.140 | 1.681 | 1.625 | 1.789 | 1.249 | 1.109 | 1.245 |

Note: T = transverse; L = longitudinal.

Table 7b

Displacement comparison between the EDS-1 skew bridge and their equivalent non-skew bridges for increased periods

| Ductility | Case 1: Skew 30° | | Case 2: Skew 30° | | Case 3: Skew 30° | |
|-----------|------------------|------------|------------------|------------|------------------|------------|
| | Longitudinal | Transverse | Longitudinal | Transverse | Longitudinal | Transverse |
| 2 | 3.71% | 2.19% | 2.61% | 18.55% | -6.84% | 4.73% |
| 3 | -2.57% | 3.57% | -3.98% | 14.24% | -4.88% | 4.45% |
| 4 | -4.45% | 2.48% | -8.94% | 10.00% | -5.05% | 5.15% |
| 5 | -9.55% | -2.85% | -6.60% | 10.22% | -7.69% | 2.23% |
| 6 | -10.52% | -5.79% | -3.34% | 6.40% | -11.24% | -0.29% |

Table 8a

Displacement comparison between the non-skew bridges with EDS-1 and EDS-2 of period 0.2 s

| Ductility Demand μ | Displacement Limit (in) | Displacement demand of EDS-1 nonskew bridge (in) | Displacement demand of EDS-2 nonskew bridge (in) | Difference [(EDS-2/EDS-1)-1] |
|------------------------|-------------------------|--|--|------------------------------|
| 2 | 0.417 | 0.391 | 0.385 | -1.53% |
| 3 | 0.626 | 0.662 | 0.699 | 5.59% |
| 4 | 0.834 | 0.983 | 1.049 | 6.71% |
| 5 | 1.043 | 1.336 | 1.368 | 2.40% |
| 6 | 1.251 | 1.637 | 1.628 | -0.55% |

Table 8b

Displacement demands of the skew bridge with EDS-2 corresponding to equivalent non-skew bridges of period 0.2 s (Unit: in).

| Ductility | Skew 15° | | Skew 30° | | Skew 45° | | Skew 60° | | Skew 75° | |
|-----------|----------|--------|----------|--------|----------|--------|----------|--------|----------|--------|
| | Longi. | Trans. |
| 2 | 0.474 | 0.455 | 0.430 | 0.445 | 0.382 | 0.398 | 0.362 | 0.385 | 0.368 | 0.385 |
| 3 | 0.830 | 0.850 | 0.761 | 0.768 | 0.668 | 0.697 | 0.640 | 0.651 | 0.624 | 0.633 |
| 4 | 1.183 | 1.292 | 1.102 | 1.170 | 0.978 | 1.054 | 0.978 | 0.973 | 0.943 | 0.906 |
| 5 | 1.562 | 1.685 | 1.399 | 1.549 | 1.298 | 1.432 | 1.317 | 1.358 | 1.268 | 1.229 |
| 6 | 1.948 | 2.073 | 1.674 | 1.883 | 1.599 | 1.729 | 1.605 | 1.685 | 1.531 | 1.543 |

Table 8c

Displacement comparison between the skew bridge with EDS-2 and their equivalent non-skew bridges of period 0.2 s.

| Ductility | Skew 15° | | Skew 30° | | Skew 45° | | Skew 60° | | Skew 75° | |
|-----------|----------|--------|----------|--------|----------|--------|----------|--------|----------|---------|
| | Longi. | Trans. |
| 2 | 23.15% | 18.24% | 11.82% | 15.68% | -0.66% | 3.48% | -6.07% | 0.05% | -4.31% | 0.14% |
| 3 | 18.73% | 21.64% | 8.91% | 9.87% | -4.44% | -0.30% | -8.41% | -6.90% | -10.69% | -9.43% |
| 4 | 12.77% | 23.14% | 4.97% | 11.51% | -6.79% | 0.44% | -6.76% | -7.30% | -10.18% | -13.65% |
| 5 | 14.19% | 23.12% | 2.29% | 13.20% | -5.12% | 4.64% | -3.74% | -0.75% | -7.31% | -10.17% |
| 6 | 19.63% | 27.30% | 2.79% | 15.65% | -1.80% | 6.18% | -1.45% | 3.46% | -5.96% | -5.25% |

Table 9a

Displacement demands of the skew bridge and their equivalent non-skew bridges with EDS-2 of increased periods (Unit: in).

| Ductility | Case 1 | | | Case 2 | | | Case 3 | | |
|-----------|----------|-------|-------|----------|-------|-------|----------|-------|-------|
| | Non-skew | | Skew | Non-skew | | Skew | Non-skew | | Skew |
| | L&T | L | T | L&T | L | T | L&T | L | T |
| 2 | 0.359 | 0.333 | 0.334 | 0.496 | 0.481 | 0.487 | 0.426 | 0.421 | 0.387 |
| 3 | 0.544 | 0.517 | 0.516 | 0.872 | 0.832 | 0.823 | 0.634 | 0.651 | 0.610 |
| 4 | 0.805 | 0.762 | 0.727 | 1.186 | 1.176 | 1.165 | 0.851 | 0.862 | 0.833 |
| 5 | 1.056 | 0.994 | 0.940 | 1.519 | 1.469 | 1.436 | 1.102 | 1.068 | 1.033 |
| 6 | 1.305 | 1.218 | 1.150 | 1.847 | 1.753 | 1.665 | 1.343 | 1.273 | 1.232 |

Note: T = transverse; L = longitudinal.

Table 9b

Displacement comparison between the EDS-2 skew bridge and their equivalent non-skew bridges for increased periods

| Ductility | Case 1: Skew 30° | | Case 2: Skew 30° | | Case 3: Skew 30° | |
|-----------|------------------|------------|------------------|------------|------------------|------------|
| | Longitudinal | Transverse | Longitudinal | Transverse | Longitudinal | Transverse |
| 2 | -7.30% | -6.90% | -3.12% | -1.94% | -1.11% | -9.12% |
| 3 | -5.00% | -5.15% | -4.54% | -5.60% | 2.54% | -3.83% |
| 4 | -5.41% | -9.72% | -0.84% | -1.72% | 1.36% | -2.13% |
| 5 | -5.83% | -10.91% | -3.26% | -5.43% | -3.11% | -6.30% |
| 6 | -6.62% | -11.78% | -5.07% | -9.83% | -5.16% | -8.20% |

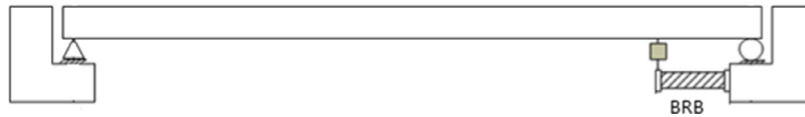


Fig. 8. Simplified bridge model with BRB connecting the bridge abutment and girder.

changes. The required minimum length of the BRB located across an expansion joint can then be selected such that the BRB's low cycle fatigue life exceeds the bridge design life of 75 years specified by AASHTO [9]. Longitudinal BRBs shorter than this length would need to be designed in series with lock-up devices that allow thermal expansion; alternatively, the BRBs could be scheduled to be replaced before they reach their expected fatigue life.

To consider the variability in temperature yearly fluctuations across North America, 9 cities in seismic regions were arbitrarily chosen to investigate a wide range of temperature variations within a year. They are Anchorage, Alaska; Boston, Massachusetts; Charleston, South Carolina; Los Angeles, California; Memphis, Tennessee; Portland, Oregon; San Francisco, California; Seattle, Washington, and; Quebec City, Canada. For each of those cities, daily temperature data were collected from Accuweather [32] as shown in Fig. 9. Recorded maximum and minimum temperatures within a day were transformed into strain histories for BRBs. Calculation of strain histories require specifying a reference temperature T_r , defined as the temperature when the BRB was first installed. Analyses were conducted considering a number of reference temperatures, ranging between the maximum and minimum temperature at each bridge location, at intervals of 10 °F. Note that the strains caused by the temperature-induced displacement history can be considered to concentrate over the length of the yielding core plate, as the rest of the BRB has much larger cross section area. Therefore, the ratios of BRB yielding core plate length over total bridge length is what was actually considered in calculating BRB thermal strain and fatigue life, which were taken as 0.5% to 3% at intervals of 0.5% for each location. Fig. 10 shows the resulted strain and stress-strain hysteresis for a BRB installed in a bridge in Memphis, Tennessee at different reference temperatures of 30 and 100 °F, when the BRB's core plate length ratio is assumed to be 0.5% of the total bridge length.

The software program *Fatiga Version 1.03* [33] was chosen to calculate low cycle fatigue life using the strain history and the fatigue properties of the BRB core plate material (ASTM A36 steel). The resulting strain histories were characterized as variable amplitude strain loading (because the amplitude of the strain ranges changed in each cycle instead of being of constant amplitude). Strain cycles were obtained using the Rainflow Counting method and the damage (i.e., the percentage of the total fatigue life) caused by cycles at each stress-range amplitude were accumulated using Miner's rule. The Smith-Watson and Topper [34] method was used to calculate fatigue life, considering the tensile mean stress effect. The damage done by all cycles in the temperature-induced strain history (i.e., for one year) can be obtained. Since the BRB fails when the cumulative damage reaches 1.0, therefore, the fatigue life is the reciprocal of the damage caused by the strain history for one year (i.e., a single application of the temperature-induced strain history). In other words, the fatigue life is the number of times that this strain history can be applied to the BRB before it fails.

In places where the yearly fluctuations of temperature were more severe (the most severe case being Memphis for the cities considered), the calculated fatigue life of the BRB was less compared to places where the yearly temperature variations were smaller. In general, a minimum BRB's yielding core plate length ratio of 3% proved to be sufficient to avoid low-cycle fatigue of the BRB due to 75 years of thermal changes on the bridge

superstructure for all locations, for all the install temperatures and cities considered.

Note that, in this low-cycle fatigue study, the longitudinal BRB was considered to be installed horizontally aligned with the bridge longitudinal axis. However, in both the EDS-1 and EDS-2 schemes, BRBs are installed at an angle with the bridge longitudinal axis, both vertically and horizontal. Considering this geometry effect would result in smaller minimum length demands for the BRBs to satisfy their low-cycle fatigue performance requirement, as a result, the recommended minimum yielding core plate length ratio of BRB of 3% is conservative and was kept for simplicity.

However, the above estimated fatigue life of BRBs obtained from *Fatiga* is solely based on the axial strain loading applied to the core steel (for ASTM A36 steel material). Note that the core plate of a BRB typically develops local buckling under the applied low cycle fatigue strain loading (albeit of constrained amplitude). This local buckling produces additional flexural plastic deformations that add up to the pure axial strains, which was used to calculate the fatigue life. Therefore, a calibration factor was deemed necessary to account for the fact that the local buckling of BRBs may reduce the estimated low-cycle fatigue life results obtained based on metal properties.

Since little data is available for the low-cycle fatigue of BRBs under variable amplitude loading, prior to the tests conducted for this project, a tentative calibration factor was selected based on the constant amplitude loading experiments by Usami et al. [35], Wang et al. [36], Akira et al. [37] and Maeda et al. [38]. The strain history applied to the BRBs up to failure in those tests was input to *Fatiga* to get the estimated fatigue life of each tested BRB. The damage calculated by *Fatiga* for each of these tests to failure is essentially equal to the calibration factor. Based on those results, the calibration factor was found to vary with the strain magnitude, ranging from 0.05 to 0.53. Note that this calibration factor is also expected to depend on how the BRB is fabricated, as this would have an impact on the amplitude of the local buckles in the BRB core. Therefore, the minimum BRB's yielding core plate length ratio that is sufficient to avoid low-cycle fatigue of the BRB for 75 years of thermal changes on the bridge superstructure could be larger than 3%. Note that this value is subject to change if implemented at locations with more critical thermal variations than considered in the study.

8. Conclusions

Design equations for two types of bidirectional ductile diaphragms used as EDSs were proposed for both skew and non-skew bridges. The approach was taken to design the skew bridges to have the same yield strength and yield displacement in the transverse and longitudinal directions as their equivalent non-skew bridges. Parametric nonlinear time history analyses were performed on the skew and non-skew bridge with both EDSs configurations to examine their seismic performance. And the resulted inelastic displacement demands of non-skew and skew bridges with both types of EDSs were compared with the elastic spectral displacements of non-skew EDS-1 bridge in both the longitudinal and transverse directions, to obtain the magnification factors R_{d1} and R_{d2} . It was found that the displacement demands of EDSs for a given bridge, $\delta_y \mu R_{d1} R_{d2}$, can be predicted and used to obtain the

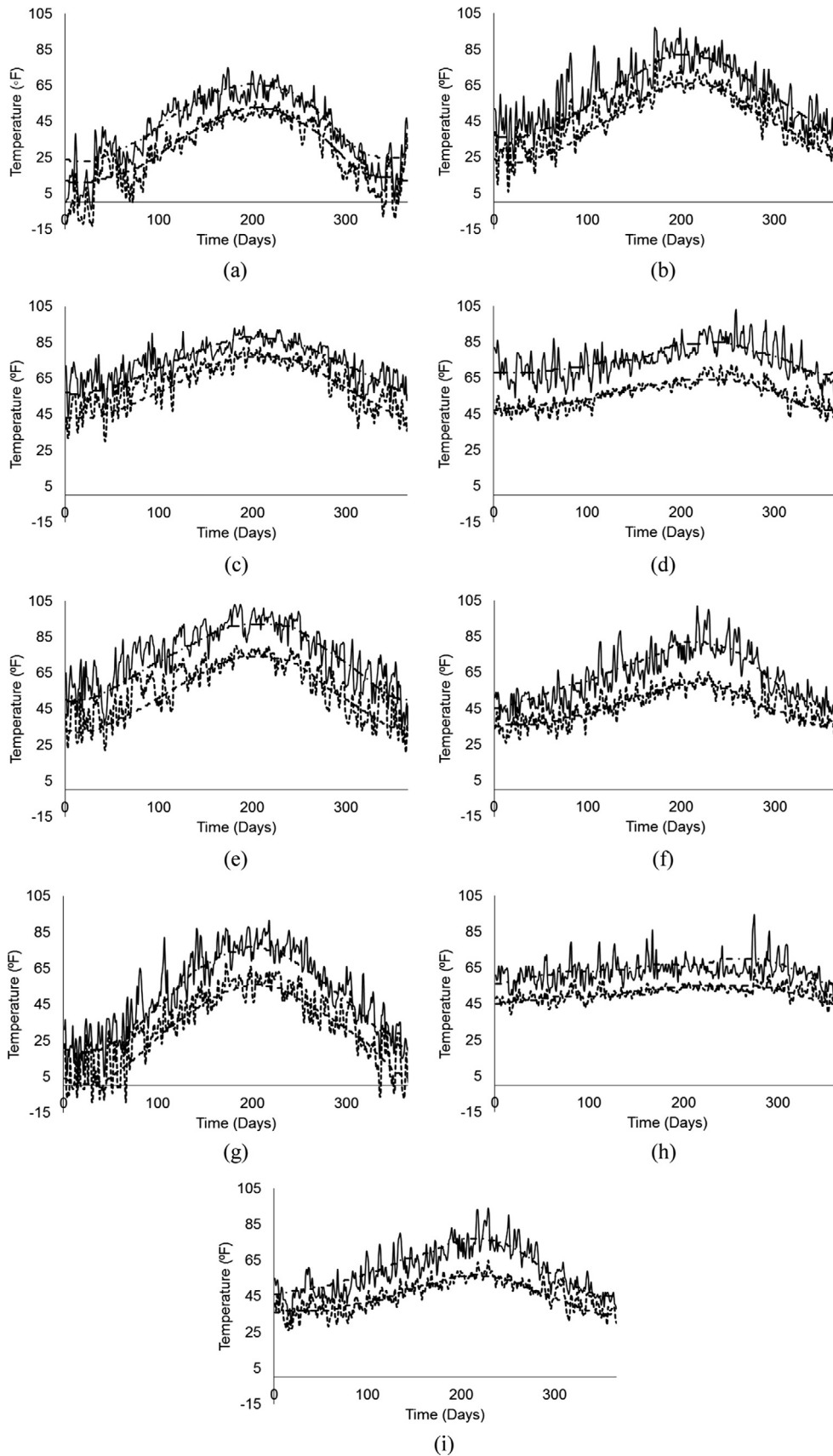


Fig. 9. Recorded temperature at selected locations: a) Anchorage, Alaska; b) Boston, Massachusetts; c) Charleston, South Carolina; d) Los Angeles, California; e) Memphis, Tennessee; f) Portland, Oregon; g) Quebec City, Canada; h) San Francisco, California; i) Seattle, Washington.

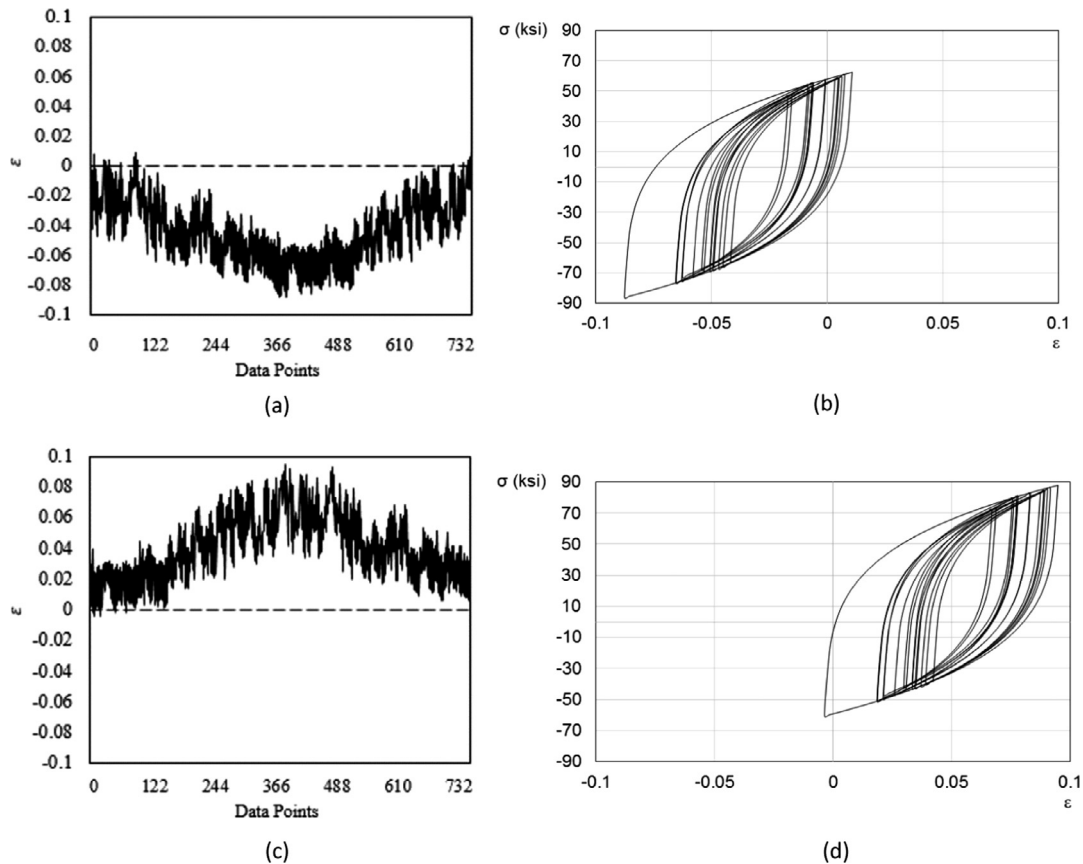


Fig. 10. Strain history and corresponding stress-strain hysteresis of BRBs in a bridge located in Memphis, TN (BRB core plate length/bridge length = 1%): (a) strain history at $T_r = 30\text{ }^\circ\text{F}$; (b) stress-strain hysteresis at $T_r = 30\text{ }^\circ\text{F}$; (c) strain history at $T_r = 100\text{ }^\circ\text{F}$; (d) stress-strain hysteresis at $T_r = 100\text{ }^\circ\text{F}$.

required relative end displacement of the BRB. To avoid the low-cycle fatigue problem BRBs installed across expansion joints and subjected to bridge thermal expansion histories, a minimum ratio of 3% for the BRB's yielding core length's ratio over the whole bridge length was recommended. From these analytical results, both the seismic end-displacement demands and the length ratio limit of the BRB can be used to design the BRBs to ensure the desired ductile bidirectional performance of the EDSs.

Acknowledgments

This study was sponsored by the Transportation Research Board of the National Academies under the TRB-IDEA Program (NCHRP-172). The authors thank Lian Duan from the California Department of Transportation, who served as the NCHRP IDEA Project Advisor, and the other members of the Project's Expert Advisory Panel, namely Geoffrey Swett and Bijan Khalegi from the Washington Department of Transportation, Taneja, Rajesh and Richard Marchione from the New York Department of Transportation, Tom Ostrom from the California Department of Transportation, and Phil Yen and Fred Faridazar from the Federal Highway Administration, for their valuable comments and oversight in this project. However, any opinions, findings, conclusions, and recommendations presented in this report are those of the writers and do not necessarily reflect the views of the sponsor.

References

- [1] Zahrai SM, Bruneau M. Impact of diaphragms on seismic response of straight slab-on-girder steel bridges. *ASCE J Struct Eng* 1998;124(8):938–47.
- [2] Zahrai SM, Bruneau M. Ductile end-diaphragms for the seismic retrofit of slab-on-girder steel bridges. *ASCE J Struct Eng* 1999;125(1):71–80.
- [3] Zahrai SM, Bruneau M. Cyclic testing of ductile end-diaphragms for slab-on-girder steel bridges. *ASCE J Struct Eng* 1999;125(9):987–96.
- [4] Sarraf M, Bruneau M. Ductile seismic retrofit of steel deck-truss bridges. I: strategy and modeling. *ASCE J Struct Eng* 1998;124(11):1253–62.
- [5] Sarraf M, Bruneau M. Ductile seismic retrofit of steel deck-truss bridges. II: design applications. *ASCE J Struct Eng* 1998;124(11):1263–71.
- [6] Bruneau M, Sarraf M, Zahrai SM, Alfawakhiri F. displacement-based energy dissipation systems for steel bridges diaphragms. *J Constr Steel Res* 2002;58(5–8):801–17.
- [7] Carden LP, Itani AM, Buckle JG. Seismic performance of steel girder bridges with ductile cross frames using single angle X braces. *J Struct Eng ASCE* 2006;132(3):329–37.
- [8] Carden LP, Itani AM, Buckle JG. Seismic performance of steel girder bridges with ductile cross frames using buckling-restrained braces. *J Struct Eng ASCE* 2006;132(3):338–45.
- [9] AASHTO. American Association of State Highway and Transportation Officials. 2nd. Washington, DC: AASHTO Guide Specifications for LRFD Seismic Bridge Design; 2011.
- [10] Celik O, Bruneau M. Skewed slab-on-girder steel bridge superstructures with bidirectional-ductile end diaphragms. *ASCE J Bridge Eng* 2011;16(2):207–18.
- [11] Wada A, Huang YH, Iwata M. Passive damping technology for buildings in Japan. *Prog Struct Eng Mater* 2000;2(3):335–50. John Wiley & Sons Ltd.
- [12] Aiken ID, Clark PW, Tajirian, FF, Kasai K, Kimura I, Ko E. Unbonded braces in the united states – design studies, large-scale testing and the first building application. In: Proceedings, Japan Passive Control Symposium, Tokyo Institute of Technology, Japan; 2000.
- [13] Clark P, Aiken I, Kasai K, Kimura I. Large-scale testing of steel unbonded braces for energy dissipation. In: Proceedings of the Structural Congress, Philadelphia, Pennsylvania; 2000.
- [14] Lopez W, Gwie D, Saunders M, Lauck T. Lessons learned from large-scale tests of unbonded braced frame subassemblage. In: Proceedings 71st Annual Convention, Structural Engineers Association of California, Sacramento, California; 2002. p. 171–183.
- [15] Usami T, Lu Z, Ge H. A seismic upgrading method for steel arch bridges using Buckling-Restrained Braces. *Earthquake Eng Struct Dynam* 2005;34(4–5):471–96.
- [16] Kanaji H, Kitazawa M, Suzuki N. Seismic retrofit strategy using damage control design concept and the response reduction effect for a long-span truss bridge. *US-Japan Bridge Workshop*; 2005.
- [17] Reno M, Pohl M. Seismic retrofit of California's auburn-foresthill bridge. *J Transp Board TRB* 2010;2201(2010):83–94.

- [18] Oya T, Fukasawa T, Fujiwara, M. et al. Practical study on a new type Buckling-Retrained-Brace. In: Proceeding of the International Association for Shell and Spatial Structure (IASS) Symposium 2009, Valencia; 2009.
- [19] Lanning J, Benzoni G, Uang CM. Using buckling-restrained braces on long-span bridges. i: full-scale testing and design implications. *J Bridge Eng* 2016. [http://dx.doi.org/10.1061/\(ASCE\)BE.1943-5592.0000781.04016001](http://dx.doi.org/10.1061/(ASCE)BE.1943-5592.0000781.04016001).
- [20] Uang CM, Bruneau M, Tsai KC. Seismic design of steel bridges”, chapter in “the CRC handbook of bridge engineering - seismic design. Boca Raton, Florida: CRC Press; 2014. p. 301–36.
- [21] Wei X, Bruneau M. “Buckling restrained braces applications for superstructure and substructure protection in bridges”, technical report MCEER-16-0009. Buffalo, NY: MCEER, University at Buffalo; 2016.
- [22] Aiken ID, Mahin SA, Uriz P. Large-scale testing of buckling-restrained braced frames. In: Proc., Japan Passive Control Symp., Tokyo Institute of Technology, Tokyo; 2002. 35e44.
- [23] Roeder CW, Lehman DE, Christopoulos A. Seismic performance of special concentrically braced frames with buckling restrained braces. In: Proc., 8th U. S. National Conf. on Earthquake Engineering, Curran Associates, San Francisco; 2006.
- [24] Tremblay R, Bolduc P, Neville R, DeVall R. Seismic testing and performance of buckling-restrained bracing systems. *Can J Civ Eng* 2006;33(2). 183e198.
- [25] Tsai KC, Hsiao PC, Wang KJ, Weng YT, Lin ML, Lin KC, et al. Pseudo-dynamic tests of a full-scale CFT/BRB frame-part I: specimen design, experiment and analysis. *Earthquake Eng Struct Dynam* 2008;37(7):1081–98.
- [26] Tsai KC, Hsiao PC. Pseudo-dynamic test of a full-scale CFT/BRB frame-part II: seismic performance of buckling restrained braces and connections. *Earthquake Eng Struct Dynam* 2008;37(7):1099–115.
- [27] Hikino T, Okazaki T, Kajiwara K, Nakashima M. Out-of-plane stability of buckling-restrained braces placed in chevron arrangement. *J Struct Eng* 2013. [http://dx.doi.org/10.1061/\(ASCE\)ST.1943-541X.0000767.1812-1822](http://dx.doi.org/10.1061/(ASCE)ST.1943-541X.0000767.1812-1822).
- [28] OpenSees Version 2.4.6 [Computer software]. University of California, CA.
- [29] FEMA P-695. Quantification of building seismic performance factors. In: prepared by Applied technology council for the federal emergency management agency, Washington DC; 2009.
- [30] Miranda E, Bertero VV. Evaluation of strength reduction factor for earthquake-resistant design. *Earthquake Spectra* 1994;10(2):1994.
- [31] MCEER-ATC 49. Recommended LRFD Guidelines for the Seismic Design of Highway Bridges. Tech. Rep. MCEER-03-SP03, MCEER, Uni. at Buffalo, Buffalo, NY; 2003.
- [32] AccuWeather. Retrieved from <<http://www.accuweather.com/>>; 2012.
- [33] Fatiga Version 1.03 [Computer software]. Fatec Engineering, Bergschenhoek, Netherlands.
- [34] Smith KN, Watson P, Topper TH. A stress-strain function for the fatigue of metals. *J Mater ASTM* 1970;5:767–78.
- [35] Usami T, Wang C, Funayama J. Low-cycle fatigue tests of a type of buckling restrained braces. *Procedia Eng* 2011;14:956–64.
- [36] Wang CL, Usami T, Funayama J. Evaluating the influence of stoppers on the low-cycle fatigue properties of high-performance buckling-restrained braces. *Eng Struct* 2012;41:167–76.
- [37] Akira W. Fatigue properties of practical-scale unbonded braces. Nippon steel technical report, No.82; 2000.
- [38] Maeda Y, Nakata Y, Iwata M, Wada A. Fatigue properties of axial-yield type hysteresis dampers. *J Struct Constr Eng* 1998;503:109–15.